Article

THE ROLE OF THERMOVISCOUS AND THERMOCAPILLARY EFFECTS IN THE COOLING OF A MOLTEN FREE LIQUID FILM DRAINING DUE TO GRAVITY

Hani Nami Alahmadi [1,‡] and Shailesh Naire [2,‡*]

[1] Department of Mathematics, College of Science, Jouf University, Sakaka P.O. Box 2014, Saudi Arabia; hnalahmadi@ju.edu.sa
[2] School of Computing and Mathematics, Keele University, ST55BG, United Kingdom; s.naire@keele.ac.uk
* Correspondence: s.naire@keele.ac.uk
‡ These authors contributed equally to this work.

Abstract: We consider theoretically the two-dimensional flow in a vertically-aligned thick molten liquid film to investigate the competition between cooling and draining due to gravity, relevant in the formation of metallic foams. The molten liquid in the film cools as it drains, losing its heat to the surrounding colder air and substrate. We extend our previous model in Alahmadi *et al*. [1] to include non-isothermal effects resulting in coupled nonlinear evolution equations for the film's thickness, extensional flow speed, and temperature. The coupling between the flow and cooling is via a constitutive relationship for the temperature-dependent viscosity and surface tension. This model is parameterized by the heat transfer coefficients at the film-air free surface and film-substrate interface, the Péclet number, the viscosity-temperature coupling parameter and the slope of the linear surface tension-temperature relationship. A systematic exploration of the parameter space reveal that at low Péclet numbers, increasing the heat transfer coefficient and a gradual reduction in viscosity with temperature is conducive for cooling and can slow down the draining and thinning of the film. The effect of increasing the slope of the surface tension-temperature relationship on the draining and thinning of the film is observed to be more effective at lower Péclet numbers where surface tension gradients in the lamella region oppose the gravity-driven flow. At higher Péclet numbers, though, the surface tension gradients tend to enhance the draining flow in the lamella region resulting in the dramatic thinning of the film at late times.

Keywords: Thin film viscous flows; Thermoviscous; Thermocapillary

1. Introduction

Foams play a crucial role in a variety of applications, such as in the fabrication of metallic foams [2,3] and in the food industry (e.g., bread dough) [4]. They contribute to the mechanical properties in metallic foams enhancing their stiffness and energy absorption, ideal for applications in the automobile industry, for example. They also contribute to the texture, aroma and visual appearance in food foams [4]. Therefore, understanding the factors that influence foam structure, its stability and lifetime, is of considerable interest.

The structure in metallic foams are broadly similar to that in aqueous foams, which are characterized by a network of thin liquid films (lamellae) intertwining gas bubbles. The process of liquid drainage into the Plateau borders and consequently thinning of the lamella is important in understanding bubble collapse and in predicting the lifetime of a foam or its overall stability. This process is well-studied in aqueous foams [5] where surfactants are required to stabilize foams by reducing the surface tension of the air-liquid interface. Surfactants are not available to affect the surface tension of metallic foams, therefore, nano and micro particles are often added during the foaming process to increase the effective liquid viscosity and to slow down the drainage, thinning and rupture time [3,6,7]. In addition, during metallic foam formation, solidification by cooling of liquid metal in the

Citation: Alahmadi, H.; Naire, S. The cooling of a molten liquid film draining due to gravity. *Fluids* **2023**, *1*, 0. https://doi.org/

Received:
Revised:
Accepted:
Published:

lamella is a "race against time" [8] competing against the liquid drainage, The competition between the two then determines the overall stability and pore structure of the metallic foam. The cooling and subsequent freezing of metallic foams have received very little attention even though they are crucial in the manufacture of these foams.

Non-isothermal effects are important when there exists a strong coupling between the flow and the temperature field due to a strong dependence of the liquid properties on the temperature. The viscosity of most materials decreases with temperature. Some materials, such as glass, metallic and polymeric melts, can exhibit dramatic changes in their viscosity due to variations in temperature, e.g., cooling and solidification of silicate (or glass-like) lava flows [9]. For glasses and polymers, the surface tension can also vary with temperature (surface tension in most liquids decreases with increase in temperature), perhaps not as dramatic as the variation in viscosity.

In the context of metallic foams, the heat transfer between the hot liquid within the lamella and Plateau borders and the cooler surrounding gas bubbles via the free surface, could result in the lamella cooling down considerably and rapidly in some situations. The resulting thermoviscous (viscosity variations with temperature) and thermocapillary effects (surface tension variations with temperature) could have a significant influence on film drainage and thinning, and overall foam stability.

Indeed, Cox *et al*. [8] were the first to theoretically investigate the competition between liquid drainage and freezing in the formation of metallic foams. They combined the so-called foam drainage equation [5] with the heat conduction equation to derive a bubble coalescence criterion which allows for the rupture of thin films. Their one-dimensional model is restricted to cooling taking place only at the top and bottom surfaces, and does not account for heat loss from the air-liquid interface. Moreover, they only investigate viscosity variation with temperature but not surface tension variations. More recently, Shah *et al*. [10] have investigated the influence of thermal fluctuations on the drainage, thinning and rupture of liquid films. They show that thickness variations due to thermal fluctuations at the free surface (originating from random thermal motion of molecules) can compete with the curvature-induced drainage at the Plateau borders. In particular, if the drainage is weak, then the film ruptures at a random location due to spontaneous growth of fluctuations originating from thermal fluctuations. This is in contrast to a scenario where the drainage is strong, resulting in the film rupturing at a local depression - so-called *dimple* - between the lamella and the Plateau border. It is worth mentioning here that the role of thermoviscous and thermocapillary effects have also been investigated in a related context of extensional flow associated with the drawing of viscous threads or sheets, with focus on the stretching and pinching of the threads [11,12] or sheet rupture [13,14]. The goal of this paper is to fully investigate the coupling between the gravity-driven extensional flow and cooling without the limitations imposed by Cox *et al*. [8]. While we do not consider phase transition due to freezing, we account for cooling from both the air-liquid interface as well as the top and bottom surfaces. Moreover, we consider the influence of both thermoviscous and thermocapillary effects on the drainage and cooling of the molten liquid film.

The outline of this paper is as follows. We formulate the two-dimensional mathematical problem in §2 which provides the governing equations and boundary conditions for the flow and the temperature field. The lubrication approximation using the fact that the film's aspect ratio is small, allows simplification of the governing equations and boundary conditions to a system of three coupled PDEs for the evolution of the one-dimensional free surface shape and the extensional flow speed, and the two-dimensional temperature field. In §4, we perform numerical simulations of the evolution equations to determine the free surface shapes, the extensional flow speeds and temperature fields for a variety of parameter values related to the Péclet number, heat transfer coefficients, an exponential viscosity-temperature model and a linear surface tension-temperature model. In §5, we discuss the main results.

2. Methods

Following on from previous work [1,15], we consider the two-dimensional flow due to the draining of a liquid in a vertically-aligned film with two free surfaces and suspended between two horizontal solid frames, as shown in Fig. 1. The liquid in the film is hot, at an initial temperature $T_i^\star$, compared to its cooler surroundings at ambient temperature $T_a^\star$. The configuration shown in Fig. 1 mimics the thinning of a lamella draining into a Plateau border and is a simple idealization of a liquid foam film. Other configurations that have been investigated include a liquid film suspended over a liquid bath at its lower end [16–20]. As we will see below, it is much simpler to prescribe boundary conditions at the upper and lower ends in the configuration considered here. In addition, we assume that the film is drawn out sufficiently quickly for a stable initial film profile to exist keeping in mind that the speed at which the film is drawn will influence whether a film of specified height and thickness can be achieved and its stability [16].

The initial liquid film is sufficiently thick for gravity to play a significant role in its drainage. The liquid loses its heat via the cooler free surface at $z^\star = h^\star(x^\star, t^\star)$ (exposed to the colder air at temperature $T_a^\star$ external to the liquid film), and the top and bottom supports at $x^\star = 0, L^\star$. The flow evolves due to the effects of gravity, viscous forces and surface tension causing the liquid in the film to drain downwards in the direction of gravity and resulting in the thinning of the film. The liquid is assumed to be an incompressible and Newtonian liquid with constant properties, except, the liquid viscosity and surface tension are dependent on the temperature. We do not consider phase transition associated with solidification due to freezing near the surface or supports.The ambient temperature, $T_a^\star$ is assumed to be much higher than the melting point to prevent the film from freezing.

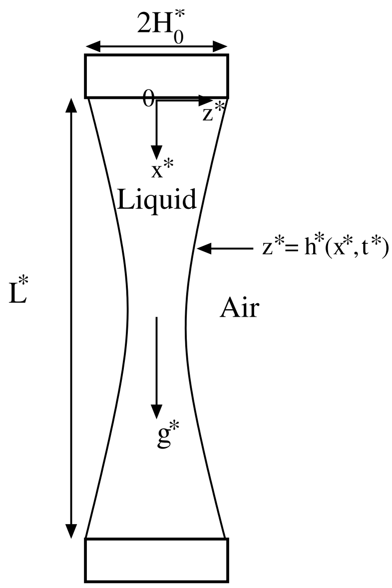

Figure 1. Schematic of a vertically-aligned two-dimensional free liquid film draining under gravity between two rigid frames (adapted from Alahmadi *et al.* [1]). The liquid within the film is hot compared to its cooler surroundings.

Figure 1 shows a schematic of the geometry. We consider a two-dimensional Cartesian coordinate system $(x^\star, z^\star)$ with the $x^\star$-axis in the vertical direction pointing downwards in the direction of the film length and the $z^\star$-axis in the horizontal direction along the film's thickness. The horizontal frames are separated by a distance $L^\star$ and are of width $2H_0^\star$. Gravity acts vertically downwards. We assume symmetry about the film's centre line at $z^\star = 0$. The two free surfaces of the film are represented by $z^\star = \pm h^\star(x, t)$. Assuming left-right symmetry, we only consider half of the film between $z^\star = 0$ and $z^\star = h^\star(x, t)$. The superscript $\star$ refers to dimensional quantities.

2.1. Governing equations

The flow is described by the Navier-Stokes equations. The density $\rho^\star$ is assumed constant (due to the incompressibility assumption), so the continuity equation reduces to

$$u^\star_{x^\star} + w^\star_{z^\star} = 0. \tag{1}$$

In the above, $\mathbf{v}^\star = (u^\star, w^\star)$ are the flow speeds in the $x^\star$ and $z^\star$ directions, respectively, and the subscript denotes differentiation with respect to the subscript variable. The momentum equations can be written as:

$$\rho^\star(u^\star_{t^\star} + u^\star u^\star_{x^\star} + w^\star u^\star_{z^\star}) = -p^\star_{x^\star} + \tau^{\star xx}_{x^\star} + \tau^{\star xz}_{z^\star} + \rho^\star g^\star, \tag{2a}$$

$$\rho^\star(w^\star_{t^\star} + u^\star w^\star_{x^\star} + w^\star w^\star_{z^\star}) = -p^\star_{z^\star} + \tau^{\star xz}_{x^\star} + \tau^{\star zz}_{z^\star}, \tag{2b}$$

where $p^\star$ is the liquid pressure, $\tau^{\star xx}$ and $\tau^{\star zz}$ are the extensional viscous stresses in the $x^\star$ and $z^\star$ directions, respectively, $\tau^{\star xz}$ is the viscous shear stress and and $g^\star$ is the acceleration due to the gravity.

The constitutive relation between the viscous stress $\boldsymbol{\tau}^\star$ and the shear rate $\dot{\boldsymbol{\gamma}}^\star$ for a Newtonian liquid with temperature-dependent viscosity is written as:

$$\boldsymbol{\tau}^\star = \mu^\star(T^\star)\dot{\boldsymbol{\gamma}}^\star, \tag{3}$$

where $\mu^\star(T^\star)$ is the temperature-dependent liquid viscosity, $T^\star$ is the temperature, and

$$\boldsymbol{\tau}^\star = \begin{pmatrix} \tau^{\star xx} & \tau^{\star xz} \\ \tau^{\star xz} & \tau^{\star zz} \end{pmatrix}, \quad \dot{\boldsymbol{\gamma}}^\star = \begin{pmatrix} 2u^\star_{x^\star} & u^\star_{z^\star} + w^\star_{x^\star} \\ u^\star_{z^\star} + w^\star_{x^\star} & 2w^\star_{z^\star} \end{pmatrix}, \tag{4}$$

The two-dimensional governing equation for the temperature, $T^\star$ in Cartesian coordinates, $(x^\star, z^\star)$ is given by

$$\rho^\star c^\star_p(T^\star_{t^\star} + u^\star T^\star_{x^\star} + w^\star T^\star_{z^\star}) = \kappa^\star[T^\star_{x^\star x^\star} + T^\star_{z^\star z^\star}], \tag{5}$$

in a material with density, $\rho^\star$, specific heat, $c^\star_p$, thermal conductivity, $\kappa^\star$ and thermal diffusivity, $\kappa^\star_d = \kappa^\star/(\rho^\star c^\star_p)$. These are assumed to be constant and independent of temperature. We neglect the contribution from viscous dissipation.

2.2. Boundary conditions

Symmetry along the center line $z^\star = 0$ is imposed through the boundary conditions:

$$w^\star = u^\star_{z^\star} = \tau^{\star xz} = T^\star_{z^\star} = 0, \text{ at } z^\star = 0. \tag{6}$$

At the free surface, $z^\star = h^\star(x^\star, t^\star)$, we have the stress boundary conditions normal and tangential to the free surface. The normal stress boundary condition balances the jump in the total normal stress (between the outside air and the liquid) with the product of the surface tension times the curvature of the free surface,

$$-p^\star + \frac{1}{1 + h^{\star 2}_{x^\star}}\left[h^{\star 2}_{x^\star}\tau^{\star xx} - 2h^\star_{x^\star}\tau^{\star xz} + \tau^{\star zz}\right] = \frac{\sigma^\star(T^\star)h^\star_{x^\star x^\star}}{\left(1 + h^{\star 2}_{x^\star}\right)^{\frac{3}{2}}}, \tag{7}$$

where $\sigma^\star(T^\star)$ is the temperature-dependent surface tension and $h^\star_{x^\star x^\star}/\left(1 + h^{\star 2}_{x^\star}\right)^{\frac{3}{2}}$ is the surface curvature. Without loss of generality, we take the atmospheric pressure to be zero, therefore, the liquid pressure $p^\star$ is relative to the atmospheric pressure. The tangential stress at the free surface for the non-isothermal case is driven by gradients in surface tension due to variations in temperature (the so-called Marangoni stress). The tangential stress boundary condition can be written as:

$$(1-h_{x^\star}^{\star 2})\tau^{\star xz}+h_{x^\star}^\star\left(\tau^{\star zz}-\tau^{\star xx}\right)=[\sigma_{x^\star}^\star(T^\star)+h_{x^\star}^\star\sigma_{z^\star}^\star(T^\star)]\sqrt{1+h_{x^\star}^{\star}{}^2}. \tag{8}$$

At the free surface, $z^\star = h^\star(x^\star, t^\star)$, we also impose a heat flux boundary condition based on Newton's law of cooling which assumes that the heat flux is proportional to the temperature difference across this boundary. This is written as:

$$-\kappa^\star \mathbf{n}^\star \cdot \nabla T^\star = a_m^\star(T^\star - T_a^\star), \tag{9}$$

where $a_m^\star$ is a heat transfer coefficient (assumed constant) and $T_a^\star$ is the ambient temperature (assumed constant), and $\mathbf{n}^\star = \frac{1}{\sqrt{1+h_{x^\star}^{\star 2}}}(-h_{x^\star}^\star, 1)$ is the outward-pointing normal vector to the free surface. We can write Eq. (9) as:

$$\kappa^\star\left(1+h_{x^\star}^{\star 2}\right)^{-\frac{1}{2}}(T_{z^\star}^\star - h_{x^\star}^\star T_{x^\star}^\star) = -a_m^\star(T^\star - T_a^\star). \tag{10}$$

Finally, the kinematic boundary condition at the free surface is given by

$$h_{t^\star}^\star = w^\star - u^\star h_{x^\star}^\star, \text{ at } z^\star = h^\star(x^\star, t^\star). \tag{11}$$

At the top and bottom boundary, $x^\star = 0, L^\star$, respectively, the film is pinned to the end of the frame and we impose no slip,

$$h^\star = H_0^\star \text{ and } \mathbf{v}^\star = 0, \text{ at } x^\star = 0, L^\star. \tag{12}$$

Here we also impose the following heat flux boundary condition:

$$-\kappa^\star \mathbf{n}^\star \cdot \nabla T^\star = b_s^\star(T^\star - T_s^\star), \tag{13}$$

$$\begin{cases} \kappa^\star T_{x^\star}^\star = b_s^\star(T^\star - T_s^\star), & \text{at } x^\star = 0, \\ -\kappa^\star T_{x^\star}^\star = b_s^\star(T^\star - T_s^\star), & \text{at } x^\star = L^\star, \end{cases} \tag{14}$$

where $b_s^\star$ is a heat transfer coefficient at the wire frames (assumed constant) and $T_s^\star$ is the temperature there (assumed constant). In the above, we have used the fact that $\mathbf{n}^\star = (-1, 0)$ at $x^\star = 0$ and $\mathbf{n}^\star = (1, 0)$ at $x^\star = L^\star$.

Using Eq. (1), and applying Leibniz's rule, one can re-write the kinematic boundary condition, Eq. (11), as

$$h_{t^\star}^\star + Q_{x^\star}^\star = 0, \;\; Q^\star = \int_0^{h^\star} u^\star(x^\star, z^\star, t^\star)\, dz^\star, \tag{15}$$

where $Q^\star(x^\star, t^\star)$ is the liquid flux at any location $x^\star$ along the length of the film. Eq. (15) represents the evolution of the film thickness, $h^\star(x^\star, t^\star)$.

The flow is coupled to the temperature field via a constitutive relationship between the viscosity and temperature, $\mu^\star(T^\star)$ and the surface tension and temperature, $\sigma^\star(T^\star)$. We assume an exponential decay in viscosity with temperature [21] and a linear dependence of surface tension on temperature [13] to describe this relationship, given by:

$$\mu^\star = \mu_{min}^\star + (\mu_0^\star - \mu_{min}^\star)e^{-\alpha^\star(T^\star - T_a^\star)}, \tag{16a}$$

$$\sigma^\star = \sigma_0^\star - M^\star(T^\star - T_a^\star), \tag{16b}$$

where $\alpha^\star$ is a temperature-viscosity coupling constant, $\mu_0^\star$ is a reference viscosity (at temperature $T_a^\star$), $\mu_{min}^\star$ is a minimum viscosity limit, $M^\star = \frac{d\sigma^\star}{dT^\star}|_{(\sigma_0^\star, T_a^\star)}$ is the rate at which surface tension depends linearly on temperature and $\sigma_0^\star$ is a reference surface tension (at temperature $T_a^\star$).

Table 1 shows the physical quantities appearing in the model including their estimates either based on aluminium foam melts where available (Tripathi *et al*. [22] and references therein) or assumed.

Table 1. Physical quantities in the model. The liquid melt properties and temperatures are based on Aluminium melts where available (Tripathi *et al.* [22] and references therein) or assumed, if otherwise.

Physical quantity	Estimated value
initial temperature, $T_i^\star$	$700 - 800^o C$
ambient temperature, $T_a^\star$	$> 660^o C$ (melting point)
temperature drop, $T_i^\star - T_a^\star$	$40 - 140^o C$ (based on melting point $660^o C$)
temperature at wire frames, $T_s^\star$	$T_a^\star$ (assumed)
density at $T_a^\star$, $\rho^\star$	$2.7 \times 10^3 \text{kg}/\text{m}^3$
viscosity at $T_a^\star$, $\mu_0^\star$	1Pa s (generally $1 - 1.4$mPa s but assumed to be enhanced by addition of particles [3,6,7]
minimum viscosity limit, $\mu_{min}^\star$	$\mu_0^\star/10$ Pa s (assumed)
surface tension at $T_a^\star$, $\sigma_0^\star$	$850 - 1100$mN/m
speciic heat capacity, $c_p^\star$	0.9kJ/kg K
thermal conductivity, $\kappa^\star$	237W/m K
thermal diffusivity, $\kappa_d^\star = \kappa^\star/(\rho^\star c_p^\star)$	$9.7 \times 10^{-5} \text{m}^2/\text{s}$
free surface heat transfer coefficient, $a_m^\star$	$1 - 10^3 \text{W}/\text{m}^2$ K (assumed)
wire frame heat transfer coefficient, $b_s^\star$	$a_m^\star$ (assumed)
temperature-viscosity coupling constant, $\alpha^\star$,	$0.01 - 0.5^o C^{-1}$ (based on viscosity drop from $\mu_0^\star$ to $\mu_{min}^\star$ in temperature range $T_i^\star$ to $T_a^\star$)
slope of surface tension-temperature relationship, $M^\star$,	$10^{-6} - 10^{-5}$ N/m$^o C$ (based on 0.01% drop in surface tension in temperature range $T_i^\star$ to $T_a^\star$)
characteristic film length, $L^\star$	10^{-2}m
characteristic film thickness, $H_0^\star$	50μm
characteristic flow speed, $U^\star = \dfrac{\rho^\star g^\star L^{\star 2}}{\mu_0^\star}$	2.7m/s
characteristic pressure, $p^\star = \rho^\star g^\star L^\star$	$270 \text{N}/\text{m}^2$
characteristic time, $t^\star = \dfrac{L^\star}{U^\star}$	4ms

2.3. *Nondimensionalization of the governing equations and boundary conditions*

We focus on the scenario where the flow is primarily extensional (or plug flow) and there is a balance between extensional viscous stresses and gravity. Following Alahmadi & Naire [1] the appropriate nondimensionalization is:

$$
\begin{aligned}
& x^\star = L^\star x, \ (z^\star, h^\star) = H_0^\star(z, h), \ (u^\star, w^\star) = \frac{\rho^\star g^\star L^{\star 2}}{\mu_0^\star}(u, \epsilon w), \\
& (p^\star, \tau^{\star xx}, \tau^{\star zz}, \tau^{\star xz}) = \rho^\star g^\star L^\star (p, \tau^{xx}, \tau^{zz}, \frac{1}{\epsilon}\tau^{xz}), \\
& (\gamma^{\star xx}, \gamma^{\star zz}, \gamma^{\star xz}) = \mu_0^\star \rho^\star g^\star L^\star (\gamma^{xx}, \gamma^{zz}, \frac{1}{\epsilon}\gamma^{xz}), \\
& t^\star = \frac{\mu_0^\star}{\rho^\star g^\star L^\star} t, \ Q^\star = \frac{\rho^\star g^\star L^{\star 2}}{\mu_0^\star} H_0^\star Q, \\
& T^\star = T_a^\star + (T_i^\star - T_a^\star)\theta, \ \ (0 \le \theta \le 1).
\end{aligned} \tag{17}
$$

$\theta = 0$, implies $T^\star = T_a^\star$ and $\theta = 1$, implies $T^\star = T_i^\star$. The ratio of the two length scales is denoted by $\epsilon = \dfrac{H_0^\star}{L^\star}$, which is typically much less than one. We are interested in deriving the thin film equations in the asymptotic limit $\epsilon \to 0$.

Substituting Eq. (17) into the governing equations and boundary conditions gives the following nondimensionalized system:

$$u_x + w_z = 0, \tag{18a}$$

$$\epsilon^2 Re(u_t + uu_x + wu_z) = -\epsilon^2 p_x + \epsilon^2 \tau^{xx}_x + \tau^{xz}_z + \epsilon^2, \tag{18b}$$

$$\epsilon^2 Re(w_t + uw_x + ww_z) = -p_z + \tau^{xz}_x + \tau^{zz}_z, \tag{18c}$$

$$Pe_r[\theta_t + u\theta_x + w\theta_z) = \epsilon^2\theta_{xx} + \theta_{zz}, \tag{18d}$$

$$\begin{pmatrix} \tau^{xx} & \tau^{xz} \\ \tau^{xz} & \tau^{zz} \end{pmatrix} = \mu(\theta)\begin{pmatrix} 2u_x & u_z + \epsilon^2 w_x \\ u_z + \epsilon^2 w_x & 2w_z \end{pmatrix}, \tag{18e}$$

$$w = u_z = \tau^{xz} = \theta_z = 0, \ \text{at} \ z = 0, \tag{18f}$$

$$\frac{\epsilon}{\hat{Ca}}\frac{\sigma(\theta)h_{xx}}{(1+\epsilon^2 h_x^2)^{\frac{3}{2}}} = -p + \frac{1}{1+\epsilon^2 h_x^2}\left[\epsilon^2 h_x^2 \tau^{xx} - 2h_x\tau^{xz} + \tau^{zz}\right], \ \text{at} \ z = h(x,t), \tag{18g}$$

$$(1-\epsilon^2 h_x^2)\tau^{xz} + \epsilon^2 h_x(\tau^{zz} - \tau^{xx}) = \frac{\epsilon}{\hat{Ca}}[\sigma_x(\theta) + h_x\sigma_z(\theta)]\sqrt{1+\epsilon^2 h_x^2}, \ \text{at} \ z = h(x,t), \tag{18h}$$

$$\theta_z = \epsilon^2 h_x\theta_x - a\epsilon^2\theta\sqrt{1+\epsilon^2 h_x^2}, \ z = h(x,t), \tag{18i}$$

$$h_t + Q_x = 0, \ \ Q = \int_0^h u(x,z,t)\, dz, \tag{18j}$$

$$h = 1, u = w = 0, \ \text{at} \ x = 0, 1, \tag{18k}$$

$$\theta_x = \epsilon^2 b(\theta - \theta_s), \ \text{at} \ x = 0, \tag{18l}$$

$$\theta_x = -\epsilon^2 b(\theta - \theta_s), \ \text{at} \ x = 1, \tag{18m}$$

$$\mu(\theta) = \mu_{min} + (1-\mu_{min})e^{-\alpha\theta}, \ \ \sigma(\theta) = 1 - \epsilon^2 M\theta. \tag{18n}$$

In the above, the dimensionless numbers $Re = \dfrac{\rho^\star {U^\star}^2/L^\star}{\mu_0^\star U^\star/{L^\star}^2}$ is the Reynolds number (compares inertial and extensional viscous forces with $U^\star = \dfrac{\rho^\star g^\star {L^\star}^2}{\mu_0^\star}$), $\hat{Ca} = \dfrac{\mu_0^\star U^\star}{\sigma_0^\star}$ is the capillary number (compares extensional viscous and surface tension forces), the reduced Péclet number, $Pe_r = \epsilon^2 Pe$, $Pe = (\rho^\star c_p^\star U^\star L^\star)/\kappa^\star = U^\star L^\star/\kappa_d^\star$, is the Péclet number (compares convective to diffusive heat transport), $\alpha = \alpha^\star(T_i^\star - T_a^\star)$ is a temperature-viscosity coupling constant, $\mu_{min} = \mu_{min}^\star/\mu_0^\star$, $M = [M^\star(T_i^\star - T_a^\star)/\sigma_0^\star]/\epsilon^2$ is the rate of decrease in surface tension with temperature, $a = a_m^\star H_0^\star/(\epsilon^2\kappa^\star)$ and $b = b_s^\star H_0^\star/(\epsilon^2\kappa^\star)$ are the heat transfer coefficients at the free surface and substrate, respectively, and $\theta_s = (T_s^\star - T_a^\star)/(T_i^\star - T_a^\star)$. We will see later on, that surface tension effects will be important over smaller lengthscales, so in anticipation of this we define a rescaled capillary number, $Ca = \dfrac{\mu_0^\star U^\star}{\epsilon\sigma_0^\star} = \hat{Ca}/\epsilon$, $\hat{Ca} = O(1)$, and retain the surface tension term at leading order. We assume $(Pe_r, M, a, b) = O(1)$.

Table 2 shows the dimensionless parameters appearing in the model and their estimated values.

Table 2. Dimensionless parameters in the model and their estimated values.

Dimensionless parameters	Values
aspect ratio, $\epsilon = H_0^\star/L^\star$	5×10^{-3}
Reynolds number, $Re = \dfrac{\rho^\star U^\star L^\star}{\mu^\star}$	72
Capillary number, $\hat{Ca} = \dfrac{\mu_0^\star U^\star}{\sigma_0^\star}$	$0.27 - 2.7$
rescaled Capillary number, $Ca = \hat{Ca}/\epsilon$	$540 - 5400$
Péclet number, $Pe = U^\star L^\star/\kappa_d^\star$	10^2
reduced Péclet number, $Pe_r = \epsilon^2 Pe$	2.5×10^{-3}
temperature-viscosity coupling, $\alpha = \alpha^\star(T_i^\star - T_a^\star)$	$0.4 - 70$
minimum viscosity, $\mu_{min} = \mu_{min}^\star/\mu_0^\star$	10^{-1}
rescaled surface tension-temperature slope, $M = [M^\star(T_i^\star - T_a^\star)/\sigma_0^\star]/\epsilon^2$	$0.04 - 0.1$
rescaled heat transfer coefficients, $(a,b) = (a_m^\star, b_s^\star)H_0^\star/(\epsilon^2\kappa^\star)$	$10^{-2} - 10$
wire frame temperature, $\theta_s = (T_s^\star - T_a^\star)/(T_i^\star - T_a^\star)$	0

2.4. *The small aspect ratio,* $\epsilon = \dfrac{H_0^\star}{L^\star} \ll 1$*, approximation*

We exploit the fact that $\epsilon = \dfrac{H_0^\star}{L^\star} \ll 1$ and expand each of the unknowns variables $(u, w, p, \tau^{xx}, \tau^{zz}, \tau^{xz})$ as a power series in ϵ^2 of the form:

$$(u, w, p, \tau^{xx}, \tau^{zz}, \tau^{xz}, \theta) = (u, w, p, \tau^{xx}, \tau^{zz}, \tau^{xz}, \theta)_0(x, z, t) + \epsilon^2(u, w, p, \tau^{xx}, \tau^{zz}, \tau^{xz}, \theta)_1(x, z, t) + O(\epsilon^4). \tag{19}$$

Substituting this in Eq. (18) we can sequentially solve for the $O(1)$ and $O(\epsilon^2)$ quantities, using which the PDEs and boundary conditions describing the evolution of the film's free surface $h(x, t)$ and the extensional flow speed $u_0(x, t)$ can be derived at leading order. The details of the derivation are provided in Appendix A. The system of PDEs and boundary conditions are given by: (for simplicity, we drop the subscript 0)

$$h_t + Q_x = 0, \quad Q = uh, \tag{20a}$$

$$Re\, h(u_t + uu_x) - 4\left[\mu(\theta)h_x u_x + \int_0^h (\mu(\theta)u_x)_x\, dz\right] = h\left[\frac{1}{Ca}h_{xxx} + 1\right] - \frac{M}{Ca}[\theta_x + h_x\theta_z|_{z=h}], \tag{20b}$$

$$\mu(\theta) = \mu_{min} + (1 - \mu_{min})e^{-\alpha\theta}, \tag{20c}$$

$$Pe_r[\theta_t + u\theta_x + w\theta_z] = \epsilon^2\theta_{xx} + \theta_{zz}, \quad w(x, z, t) = -u_x z, \tag{20d}$$

$$\theta_z = -a\epsilon^2\theta, \text{ at } z = h(x, t), \; \theta_z = 0, \text{ at } z = 0, \tag{20e}$$

$$\theta_x = \epsilon^2 b(\theta - \theta_s), \text{ at } x = 0, \; \theta_x = -\epsilon^2 b(\theta - \theta_s), \text{ at } x = 1 \tag{20f}$$

$$h(0, t) = h(1, t) = 1, h_{xxx}(0, t) = h_{xxx}(1, t) = -Ca, \tag{20g}$$

$$u(0, t) = u(1, t) = 0. \tag{20h}$$

The boundary conditions in Eq. (20g,20h) correspond physically to the film being pinned at the top and bottom (first two boundary conditions in Eq. (20g)), and no flux out of the rigid wire supports, so $Q = 0$, (represented by the last two boundary conditions in Eq. (20g) and boundary conditions in Eq. (20h)). As a consequence of this, both u and u_x are forced to be zero near the ends and the film evolves to quasi-static shapes there. We also retain the $O(\epsilon^2)$ term in Eq. (20d) in order to satisfy the boundary conditions for θ at $x = 0, 1$ (boundary conditions in Eq. (20f)).

3. Numerical methods

Equations (20a,20b) for $h(x,t)$ and $u(x,t)$, respectively, are solved for $x \in [0,1]$ with boundary conditions given by Eq. (20g,20h). The two-dimensional evolution equation, Eq. (20d), for the temperature, $\theta(x,z,t)$, is solved for $(x,z) \in [0,1] \times [0,h(x,t)]$ with boundary conditions given by Eq. (20e,20f). For computational convenience, it is useful to map the temperature field, $\theta(x,z,t)$, onto a rectangular domain using the change of variables $\bar{z} = z/h$. The transformed evolution equation for the temperature, $\theta(x,\bar{z},t)$ is solved for $(x,\bar{z}) \in [0,1] \times [0,1]$. The transformed evolution equations for h, u and θ are given by Eqs. (A22,A23) shown in Appendix B. In what follows, we drop the bar in z with the implicit understanding that $z \in [0,1]$.

The equations are solved numerically using the Method of Lines on a uniform and fixed computational mesh in the spatial directions (x,z) **[23]**. The spatial derivatives are discretised using second-order centered finite difference schemes including a first-order upwind scheme for convection terms in the temperature equation (the terms multiplying θ_x and θ_z on the left-hand-side of Eq. (A22a)). The time derivatives appearing in the equations are kept continuous. We use the trapezoidal rule to approximate the integral in the expression for $u(x,t)$ in (A23b). The resulting system of differential-algebraic equations for the unknowns in h, u and θ at each grid point are solved in MATLAB (Release 2013a, The MathWorks Inc., Natick, Massachusetts, United States) using the stiff ODE solver *ode15i*. The corresponding computational mesh sizes were $\Delta x, z = 10^{-3} - 10^{-2}$ resulting in a system of $O(10^4 - 10^6)$ differential-algebraic equations (DAEs) required to be solved at each time step. For $Pe_r \gg 1$, the problem can have very narrow thermal boundary layers near $z = h(x,t)$ of width $O(Pe_r^{-1/2})$ and $x = 0, 1$ of width $O(\epsilon Pe_r^{-1/2})$. The smallest value of $\Delta z = 10^{-3}$ is sufficient to resolve these boundary layers for $Pe_r \leq 10^3$. For $Pe_r > 10^3$, much smaller values of $\Delta x, z$ are required which increases the number of DAEs at each time step, hence the computational effort. These results are not shown here as they are not different from the $Pe_r = 10^3$ results. The time step was controlled within the solver to maintain the stability of the numerical solutions. The accuracy and convergence of the numerical scheme are formally checked by systematically reducing the mesh sizes $\Delta(x,z)$ for sample cases corresponding to a low, intermediate and high reduced Péclet number Pe_r. Based on this, we can confirm that for the mesh sizes stated above the numerical solutions presented below are an accurate reflection of the draining process.

4. Results

We seek numerical solutions of the evolution of the film thickness $h(x,t)$, extensional flow speed $u(x,t)$ and temperature $\theta(x,z,t)$, by varying the key parameters: the reduced Péclet number Pe_r (or Péclet number Pe), rate of linear decrease in surface tension with temperature, M, the heat transfer coefficients, a, b, at the free surface and substrate, respectively, and the temperature-viscosity coupling constant, α. Table 2 provides a range of values for the dimensionless parameters. We do not always restrict the choice of the values of these parameters to be based on Table 2, but allow for a full range of realistic values to be explored in (Pe_r, M, a, b, α) space. We consider variations in the above parameters for $Ca = 10^3$ (representative of $Ca \gg 1$) and $Re = 0$. $Re \ll 1$ has no significant influence on the evolution of the film and the extensional speed, hence we choose $Re = 0$. Additionally, we choose the heat transfer coefficient at the top and bottom ends, $b = 0$, focusing on a, the heat transfer at the free surface only. The initial condition is $h(x,0) = \theta(x,z,0) = 1$ and the corresponding initial condition for the extensional flow speed is $u(x,0) = x(1-x)/8$ obtained by solving Eq. (20b) for $(h,\theta) = 1$ and $Re = 0$.

We first investigate the influence of viscosity varying with temperature, and take the surface tension to be constant (so, $M = 0$). The solid curves in Fig. 2(a,e) show the evolution of $h(x,t)$ ($h(x,t)$ is plotted on a logarithmic scale) for $t = 0 - 160$ (in steps of 20) with $\mu = 1$ (or $\theta = 0$ everywhere corresponding to a film with liquid at the ambient temperature, $T_a^\star$) and $\mu_{min} = 5 \times 10^{-2}$ (or $\theta = 1$ corresponding to a film with liquid at a hotter temperature, $T_i^\star$ everywhere), respectively. Both these cases are isothermal with differing liquid viscosities. The solid curves in Fig. 2(b, f) show the extensional speed $u(x, t)$ corresponding to $\mu = 1, \mu_{min}$, respectively. The remaining curves in Fig. 2(a, c, e) show the evolution of $h(x, t)$ ($h(x, t)$ is plotted on a logarithmic scale) for $t = 0 - 160$ (in steps of 20) for $Pe_r = 10^{-1}, 10, 10^2, 10^3$, respectively, with fixed $\alpha = 2$, $a = 0.02$, $Ca = 10^3$ and $Re = 0$. Fig. 2(b, d, f) show the corresponding evolution of $u(x, t)$, respectively.

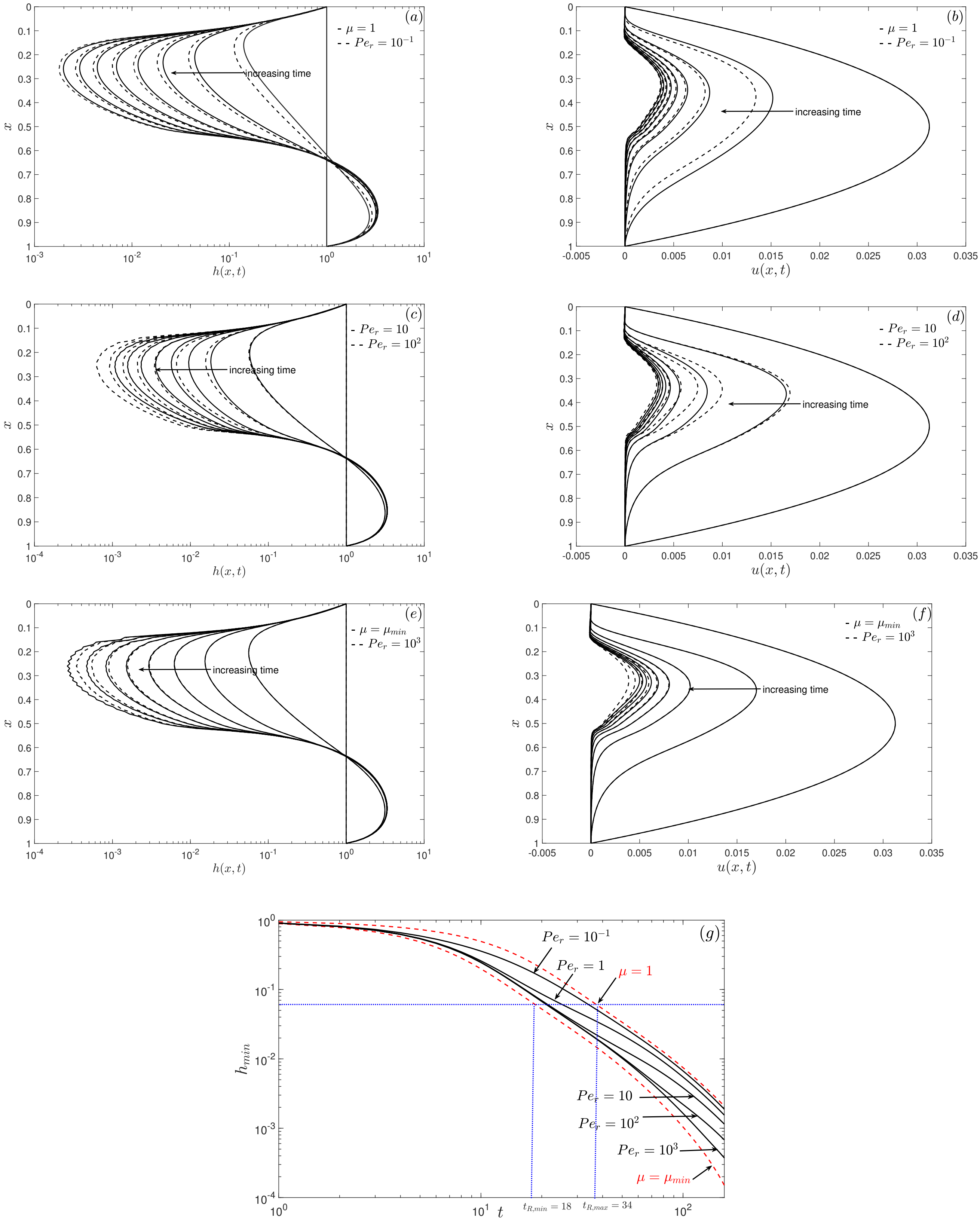

Figure 2. The evolution of the film thickness $h(x,t)$ (on a logarithmic scale) for t varying between $t = 0 - 160$ (in steps of 20) corresponding to (a) $\mu = 1$ (solid curves; isothermal case with $\theta = 0$ everywhere) and $Pe_r = 10^{-1}$ (dashed curves), (c) $Pe_r = 10$ (solid curves) and $Pe_r = 10^2$ (dashed curves) and (e) $Pe_r = 10^3$ (dashed curves) and $\mu = \mu_{min} = 5 \times 10^{-2}$ (solid curves; isothermal case with $\theta = 1$). The corresponding extensional flow speed $u(x,t)$ is shown in (b, d, f). The evolution (g) of the global minimum h_{min} as a function of time t for varying Pe_r. The parameter values are: $\alpha = 2$, $a = 0.02$, $Ca = 10^3$ and $Re = 0$.

At early times, the fluid in the film drains downwards leading to thinning of the film in the upper region and a thickening in the lower region, and the film shape is concave-out (Fig. 2(a,c,e); see also the outline profile for h shown in the leftmost panel in Fig. 3(a,d,g,j)). At late times, the fluid has drained significantly towards the lower end of the domain forming a quasi-static pendant drop there, leaving a very thin and almost flat film (lamella) in the middle region, and a quasi-static capillary meniscus at the upper end (Fig. 2(a,c,e); see also the outline profile for h shown in the rightmost panel in Fig. 3(c,f,i,l)). This late-time behaviour can be clearly observed using a logarithmic scale for $h(x,t)$ shown in Fig. 2(a,c,e). This shows the middle lamella region connecting onto quasi-static curves at the top and bottom represented by the capillary meniscus and the pendant drop, respectively. The maximum flow speeds are in the middle lamella section of the film (Fig. 2(b,d,f)) which causes the film thickness to decrease severely there. The flow speed is zero near the top in the capillary meniscus region, and at the bottom in the pendant drop region.

For small Pe_r (dashed curves in Fig. 2(a)), the cooling is significant over the entire film resulting in the temperature quickly dropping to its equilibrium value, $\theta = 0$ (or $T^\star = T_a^\star$) and the evolution of $h(x,t)$ is similar to that of isothermal draining with $\mu(\theta) = 1$ (dashed curves in Fig. 2(a)). For intermediate Pe_r (Fig. 2(c) with $Pe_r = 10, 10^2$, respectively), the cooling is less uniform and pronounced in the thinner lamella section of the film while the temperature is much higher in the thicker pendant drop and upper meniscus regions; the overall viscosity of the liquid is lower than that for low Pe_r leading to faster extensional flow speed as Pe_r increases (Fig. 2(d)) and hence faster draining and thinning of the lamella region. For much larger Pe_r (dashed curves in Fig. 2(d,e) with $Pe_r = 10^3$), the cooling is confined in a skin near the film's free surface (a diffusive boundary layer) and a collar of cooler liquid forms in the lamella region, with the rest of the liquid within the film insulated at a higher temperature $\theta \approx 1$. This results in a much lower overall viscosity, and consequently faster draining and thinning compared to lower values of Pe_r. The evolution of $h(x,t)$ is almost indistinguishable from that of isothermal draining with $\mu(\theta) = \mu_{min}$ (solid curves in Fig. 2(e)).

Fig. 2(g) tracks the evolution of the minimum in h, h_{min}, as a function of t for Pe_r between $10^{-1} \leq Pe_r \leq 10^3$. h_{min} is representative of the thickness of the lamella film region. We observe increased thinning of the minimum film thickness, $h_{min}(t)$, as Pe_r increases. As Pe_r increases the fluid drains more quickly which causes the middle section to become thinner sooner, therefore more likely to rupture at earlier times. We also observe that h_{min} is always bounded by the two isothermal curves corresponding to $\mu(\theta) = 1, \mu_{min}$, respectively (red dashed curves in figure 2(g)) and the thinning rates for small and large Pe_r tend to these limiting rates ($\propto t^{-2.25}$) [1]. To characterise the time taken for the film to thin, we define a rupture time, t_{rupt}, as the time taken for the film to drain to a prescribed thickness. In practise, we estimate t_{rupt} to be the time taken until h_{min} reduces to 5×10^{-2} of its initial thickness. We observe that the rupture time is almost doubled as $Pe_r \to 0$.

To highlight the temperature variations within the film and the non-uniform cooling as Pe_r is increased, in Fig. 3$(a-c)$, $(d-f)$, $(g-i)$ and $(j-l)$, we show the contour plot for $\theta(x,z,t)$ at times $t = 5$ (a,d,g,j), $t = 20$ (b,e,h,k) and $t = 100$ (c,f,i,l) for $Pe_r = 1, 10, 10^2, 10^3$, respectively. The other parameter values kept fixed are: $\alpha = 2$, $a = 0.02$, $Ca = 10^3$ and $Re = 0$.

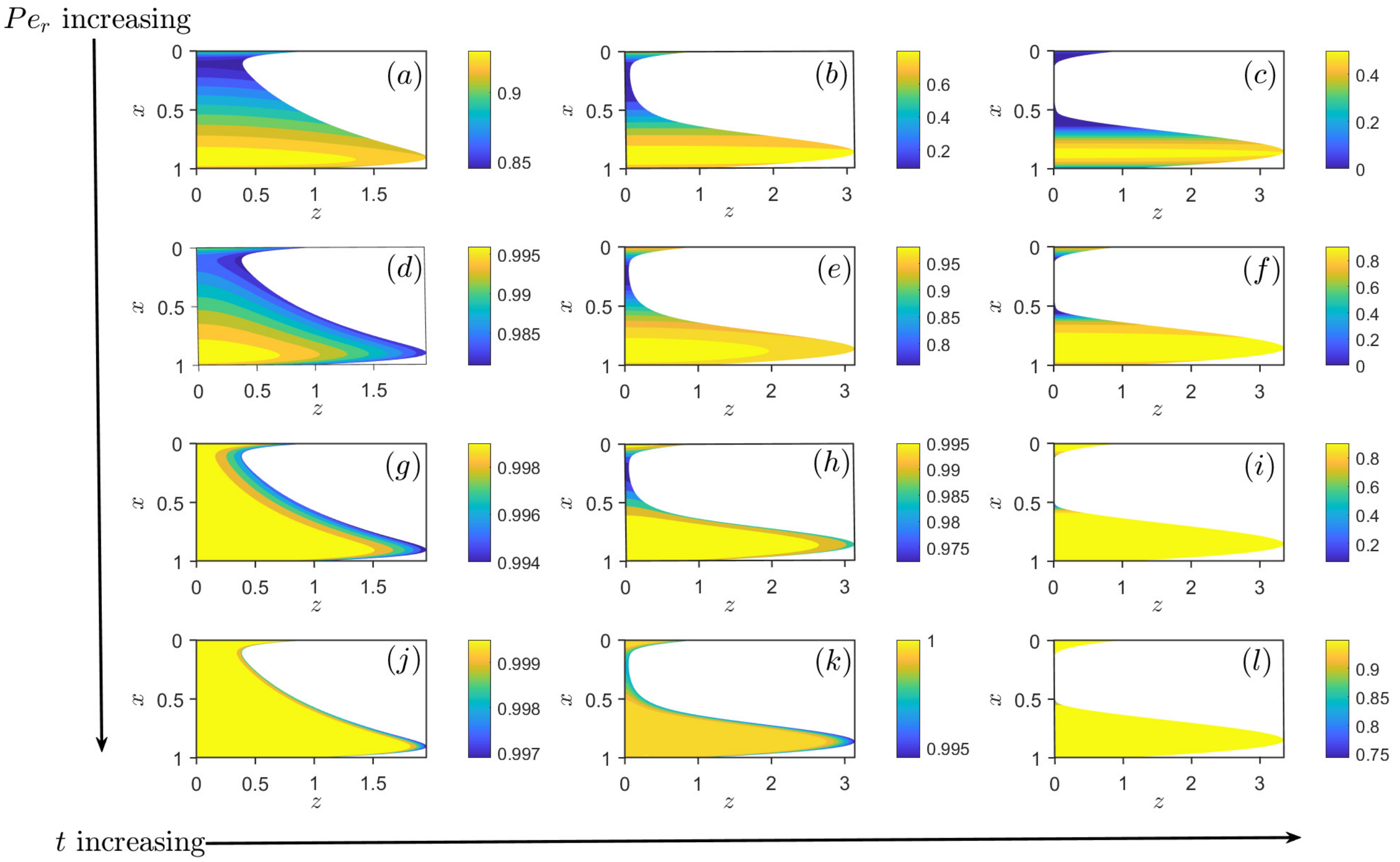

Figure 3. The contour plot for (a) $\theta(x,z,t=5)$, (b) $\theta(x,z,t=20)$ and (c) $\theta(x,z,t=100)$ for $Pe_r=1$; (d) $\theta(x,z,t=5)$, (e) $\theta(x,z,t=20)$ and (f) $\theta(x,z,t=100)$ for $Pe_r=10$; (g) $\theta(x,z,t=5)$, (h) $\theta(x,z,t=20)$ and (i) $\theta(x,z,t=100)$ for $Pe_r=10^2$; (j) $\theta(x,z,t=5)$, (k) $\theta(x,z,t=20)$ and (l) $\theta(x,z,t=100)$ for $Pe_r=10^3$. The other parameter values kept fixed are: $\alpha=2$, $a=0.02$, $Ca=10^3$ and $Re=0$.

For very small Pe_r (not shown here), the heat loss at the free surface results in the temperature dropping from its initial value $\theta=1$ ($T=T_i$) to its equilibrium value, $\theta=0$ ($T=T_a$), very quickly. At small values of Pe_r, the diffusion of temperature across the thickness of the film dominates, i.e., θ_{zz}, resulting in the film cooling uniformly. As Pe_r increases, the diffusion rate is even slower, and is less dominant in suppressing spatial variations in temperature due to non-uniform cooling both along the film (Fig. 3$(a-c)$ for $Pe_r=1$ and $(d-f)$ for $Pe_r=10$) as well as within the film (Fig. 3$(d-f)$ for $Pe_r=10$). This results in more pronounced cooling in the lamella section of the film where h is much smaller, compared to near the ends where the temperatures are much higher as h is comparatively larger there. This non-uniformity in the cooling is due to the rate of heat loss being inversely proportional to h - the thicker regions of the film retain their heat more compared to the thinner regions, which lose their heat and therefore cool relatively quickly. This non-uniformity in cooling can be clearly observed in Fig. 4(a,b) which shows the evolution of the temperature along the free surface, $\theta(x,z=h(x,t),t)$, for t varying between $t=1-160$ (in steps of 20), corresponding to $Pe_r=1,10$, respectively. For $Pe_r=1$, we observe the highest temperatures in the pendant drop region followed by the temperatures in the upper meniscus (Fig. 4(a)). For $Pe_r=10$, the highest temperatures are in the pendant drop and upper meniscus regions, and we start to observe the development of steep temperature gradients between these regions and the lamella region (Fig. 4(b)). Increasing Pe_r further, the spatial variations in θ are much more pronounced, with cooling in the middle section of the film where h is much smaller, compared to near the ends where

h is comparatively larger (Fig. 3$(g-i)$ for $Pe_r = 10^2$). At early times, we also observe variations in θ within the film (Fig. 3(g)), with the film slowly cooling from the free surface. At later times, it appears that θ is uniform across the film (Fig. 3(h,i)). The large spatial variation in θ between the ends and the lamella region is clearly observed in Fig. 4(c) which shows the evolution of the temperature along the free surface, $\theta(x, z = h(x,t), t)$, for t varying between $t = 1 - 160$ (in steps of 20), corresponding to $Pe_r = 10^2$. For even larger values of Pe_r, we clearly observe that the majority of the cooling is in the lamella section of the film, where the film is very thin; the upper capillary meniscus and the pendant drop region at the bottom remain almost insulated at its initial temperature from the cooler middle section and a thin cooler boundary layer near the free surface (Fig. 3(j,k) for $Pe_r = 10^3$ where the boundary layer is clearly visible; in Fig. 3(l) the boundary layer is very thin and not resolved here). This is also clearly identified in Fig. 4(d) which shows the evolution of the temperature along the free surface, $\theta(x, z = h(x,t), t)$, for t varying between $t = 1 - 160$ (in steps of 20), corresponding to $Pe_r = 10^3$. The significant reduction in the cooling of the middle lamella section is clearly evident at higher Pe_r. This is due to the enhanced convection of heat through the flow coming from the hotter upper meniscus region.

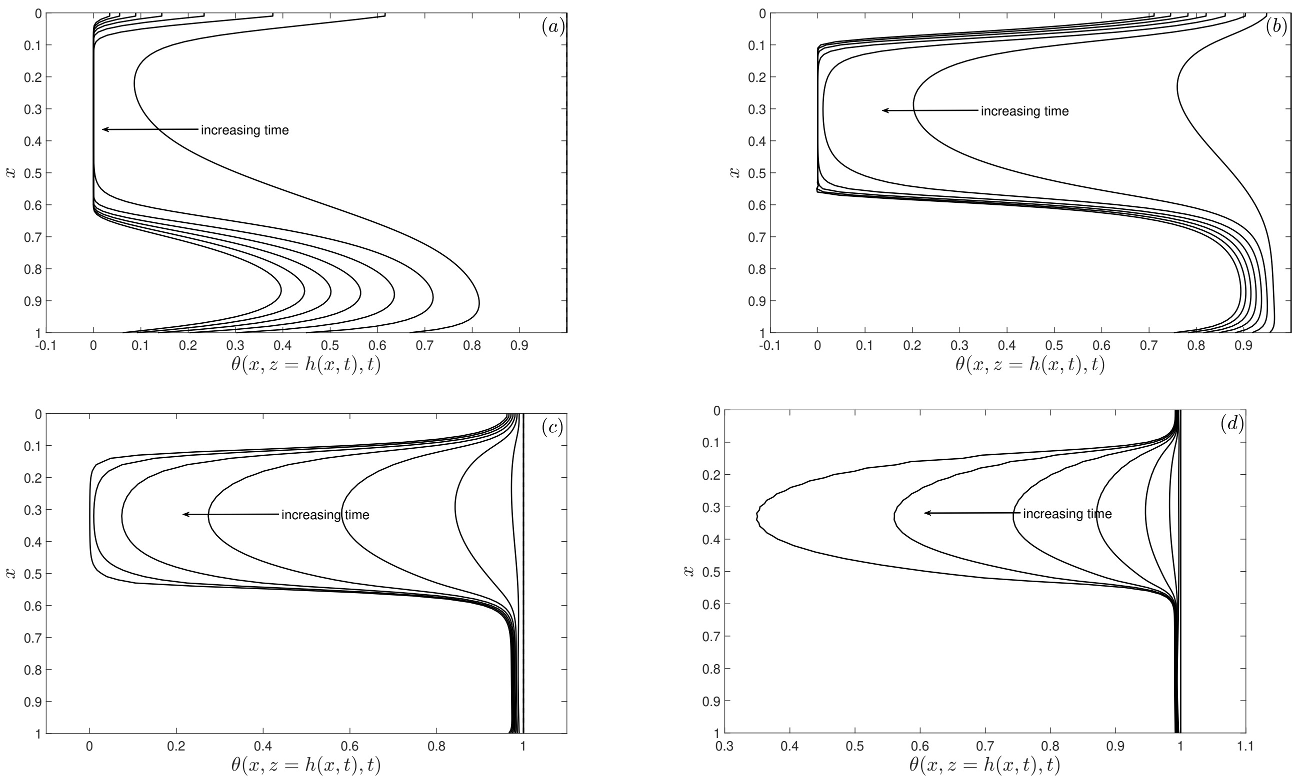

Figure 4. The evolution of the temperature at the free surface, $\theta(x, z = h(x,t), t)$ for t varying between $t = 0 - 160$ (in steps of 20) corresponding to (a) $Pe_r = 1$, (b) $Pe_r = 10$, (c) $Pe_r = 10^2$ and (d) $Pe_r = 10^3$. The other parameter values kept fixed are: $\alpha = 2$, $a = 0.02$, $Ca = 10^3$ and $Re = 0$.

Next, we investigate the influence of the viscosity-temperature decay constant α, the heat transfer coefficient at the free surface a and the surface tension-temperature parameter M on the global minimum film thickness h_{min}.

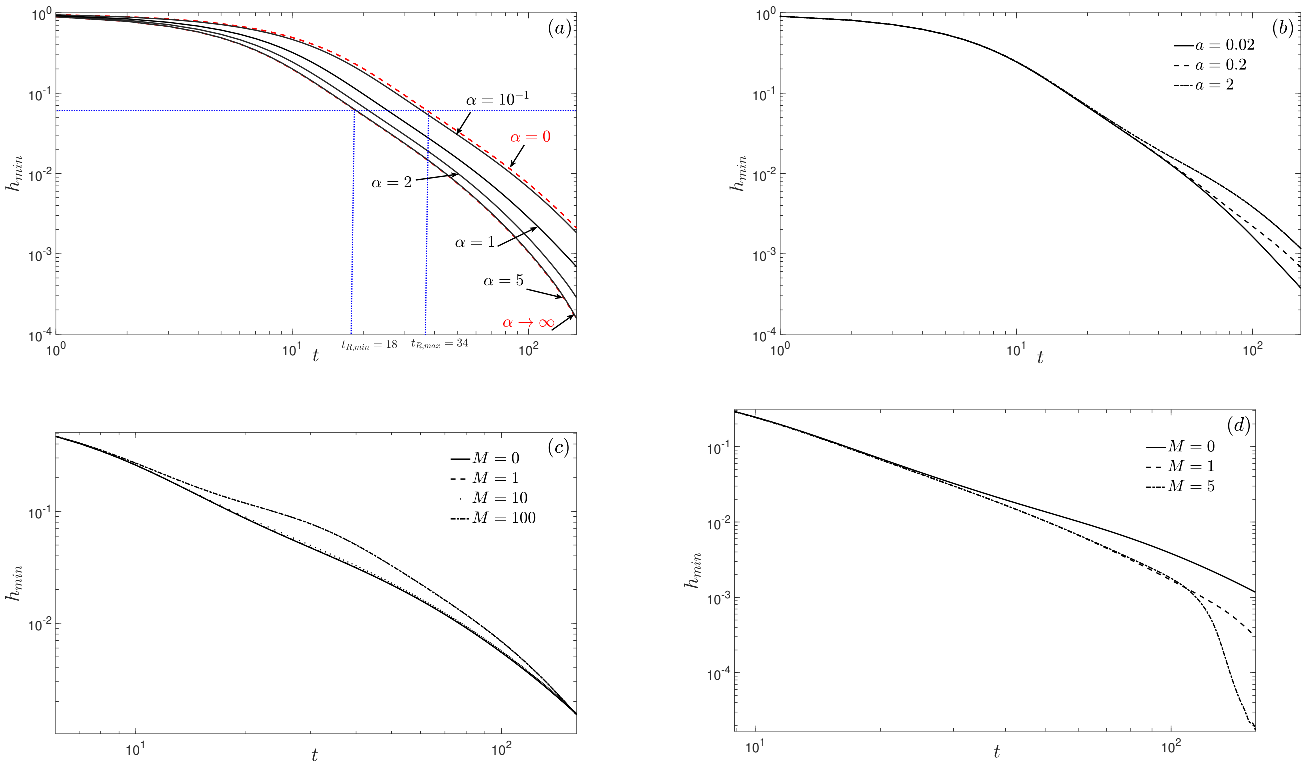

Figure 5. The global minimum h_{min} as a function of time t for (a) varying α ($Pe_r = 10^3$, $a = 0.02$), (b) varying a ($Pe_r = 10^3$, $\alpha = 2$), (c) varying M ($Pe_r = 1$, $a = 0.02$) and (d) varying M ($Pe_r = 10^3$, $a = 0.02$). The other parameter values kept fixed are $Ca = 10^3$ and $Re = 0$.

Fig. 5(a) investigates the influence of varying α on $h_{min}(t)$, for fixed $Pe_r = 10^3$ and $a = 0.02$. We observe the increased thinning of the minimum film thickness, $h_{min}(t)$, as α increases. As α increases the fluid drains more rapidly (due to the larger reduction in viscosity) which accelerates the the thinning of the middle section, therefore lowering the rupture times (by almost half the time compared to the isothermal $\mu = 1$ case). In the limit as $\alpha \to 0, \infty$, we recover the isothermal cases corresponding to $\mu = 1, \mu_{min}$ respectively (red dashed curves in Fig. 4(a)). Fig. 5(b) investigates the influence of varying a on $h_{min}(t)$, for fixed $Pe_r = 10^3$ and $\alpha = 2$. We observe the thinning of the minimum film thickness, $h_{min}(t)$, decreases as a increases. The fluid drains more slowly which slows down the thinning of the lamella section, therefore delaying the rupture times. We now study the influence of varying M on $h_{min}(t)$, for two cases corresponding to a low value of $Pe_r = 1$ (Fig. 5(c)) and a high value of $Pe_r = 10^3$ (Fig. 5(d)). We fix $\alpha = 2$ and $a = 0.02$. For low values of Pe_r, we observe h_{min} to marginally increase with M; the increase is exaggerated for larger values of M (Fig. 5(c)). This is due to gradients in surface tension generated due to variations in θ along the film (i.e., θ_x) which is much stronger in the transition region between the downstream end of the lamella region and the pendant drop compared to the transition region between its upstream end and the upper meniscus region (see Fig. 4(a)). Moreover, the stronger surface tension gradients at the downstream end of the lamella region oppose the gravity-driven flow, hence slowing down the extensional flow speed and thereby reducing the thinning of the lamella region.

In contrast, for high values of Pe_r, we observe a decrease in h_{min} at late time as M increases; the drop in h_{min} is quite dramatic for higher values of M. In this case, the surface tension gradients in the transition region between the upstream end of the lamella and the upper meniscus region are stronger than that in the transition region between its downstream end and the pendant drop region (due to θ_x being larger at the upstream end -

see Fig. 4(d)). This contribution cooperates with the gravity-driven flow, hence increasing the extensional flow speed and thereby accelerating the thinning of the lamella region.

5. Discussion

In this paper, we coupled the thin-film flow equations to a two-dimensional advection-diffusion equation for the temperature field and investigated the draining and thinning of a cooling vertically-aligned hot Newtonian liquid film for the reduced Péclet number, $Pe_r = O(1)$. We considered non-isothermal conditions which included a temperature-dependent viscosity and surface tension, and heat loss due to cooling at the free surface. A systematic parameter study revealed the influence of the system parameters on this cooling, particularly, the reduced Péclet number, Pe_r, the decay constant in the exponential viscosity-temperature model, α, the heat transfer coefficient, a, and the slope of the linear surface tension-temperature model, M. The resulting temperature and corresponding viscosity and surface tension contrast arising due to the cooling near the film's free surface significantly influenced the draining and subsequent thinning of the film.

A key contribution of this work distinguishes the thinning rate and rupture times of the lamella between the non-isothermal cases and the isothermal cases from our previous work [1]. Indeed, we have demonstrated the significant influence of cooling on these and showed that, depending on the parameter values, the lamella can thin and rupture either faster or slower than the corresponding isothermal cases (Figs. 2(g), 5).

The main highlight of our results identifies an important feature during the draining and thinning process - the preferential cooling in the film's flat middle section (lamella) compared to the top and bottom regions (Plateau borders). The rate of heat loss in the lamella is maximum due to its much smaller thickness compared to the much thicker Plateau borders (Fig. 4). The extent of this cooling was dependent on the parameter values, in particular the reduced Péclet number, Pe_r. For intermediate and large Pe_r, a draining *collar* of colder liquid was observed in the lamella sandwiched between two much hotter Plateau border regions. The hotter regions appeared to be almost insulated from the cooler middle section and a thin cooler boundary layer near the free surface (Figs. 3(i, l) and 4(c, d)). In contrast, for small values of Pe_r, the temperature isotherms are almost constant across the film thickness (Fig. 3$(a - c)$) and the film cooled almost uniformly along its thickness. The non-uniform cooling and its influence on foam film drainage identified in our work clearly suggests that it is necessary to include the heat transfer and drainage both in the lamella and Plateau borders, not considered in previous work [8]. Moreover, the cooling from the free surface is also important, again neglected in previous work which only investigated heat transfer from the solid wire frame [8]. In our model, we have assumed that the wire frames are insulated; future work will include heat transfer from both the free surface and wire frames.

We observed that the cooling rate could be enhanced by increasing the heat transfer coefficient a which slowed down the draining and thinning of the film. Moreover, a rapid drop in the viscosity with temperature controlled by the parameter α increased the draining flow and the subsequent thinning of the film. The low Pe_r limit is preferable in metallic films since the hot liquid in the film cools uniformly and rapidly, consequently the liquid viscosity increases uniformly within the film, resulting in slower drainage and thinning of the film. This can be achieved if the Péclet number, $Pe = U^\star L^\star / \kappa_d^\star$, is small (or the thermal diffusivity for the liquid, $\kappa_d^\star$, is large or the aspect ratio, ϵ, is small). For melts with low diffusivity, one would need very thin films for the low Pe_r results to be achieved. Another method to sufficiently reduce the drainage so that cooling can occur, is to disperse particles within the melt that can increase its effective viscosity, e.g., alumina particles are dispersed in aluminium foam to increase the viscosity [6,7].

Our investigations on the influence of temperature variations in surface tension showed that effect of increasing the slope of the linear surface tension-temperature relationship $M^\star$ is observed to be more effective at lower Péclet numbers where surface tension gradients in the lamella region oppose the gravity-driven flow. At higher Péclet numbers, though, the surface tension gradients tend to enhance the draining flow in the lamella region resulting in the dramatic thinning of the film at late times. Our results indicate that the thermocapillary effect has much less influence on the draining and thinning of the film in comparison to thermoviscous effects. This is due to a limitation in our model which restricts the variation in surface tension with temperature to be $O(\epsilon^2)$ in order to relegate the influence of surface tension gradients to $O(\epsilon^2)$. To accommodate larger variations in surface tension, this needs to be relaxed and a different dominant balance including surface tension gradients at leading order in ϵ needs to be explored in future.

A major limitation of this study was in not considering the influence of phase transition due to solidification which occurs when the metallic foam structure is immediately cooled to trap this foam structure in a solid. This limits our results to be only valid for temperatures much larger than the melting temperature. We were unable to investigate scenarios where, for example, a solid crust forms at the air-liquid interface (if the temperature there drops below the freezing point) on the hot draining liquid core [8]. As part of the future work, we will need to modify viscosity-temperature relationship in Eq. (16a) to model the change in viscosity at low temperatures close to when the foam is frozen, e.g., Cox *et al*. [8] choose a step function for μ that gives small values at high temperatures and high values at low temperatures. In addition, the latent heat of fusion will need to be considered. Cox *et al*. [8] use a simple specific heat-temperature relationship to mimic a peak in the specific heat around the melting temperature to represent the heat that must be absorbed before the foam solidifies. Incorporating these relationships into our model will allow us to fully describe the cooling and solidification of metallic foam films.

The theoretical framework developed here is versatile and can be readily adapted to accommodate complex melts exhibiting non-Newtonian or viscoelastic behaviour with temperature-dependent properties. This insight would form the basis for future developments of this model to utilize the results to investigate the overall behaviour of a foam network, using the framework proposed by Stewart *et al*. [24], for example.

Author Contributions: Conceptualization, Alahmadi and Naire; methodology, Alahmadi and Naire; formal analysis, Alahmadi.; investigation, Alahmadi; writing—original draft preparation, Naire; writing—review and editing, Naire; supervision, Naire. All authors have read and agreed to the published version of the manuscript.

Funding: This research received no external funding.

Data Availability Statement: The data that support the findings of this study are available from the corresponding author upon reasonable request.

Acknowledgments: This work was a part of Hani Alahmadi's PhD research at Keele University. Hani gratefully acknowledges financial support from Jouf University, the Ministry of Education, Kingdom of Saudi Arabia, and the Saudi Arabian Cultural Bureau in London (UKSACB).

Conflicts of Interest: Declare conflicts of interest or state "The authors declare no conflict of interest." Authors must identify and declare any personal circumstances or interest that may be perceived as inappropriately influencing the representation or interpretation of reported research results. Any role of the funders in the design of the study; in the collection, analyses or interpretation of data; in the writing of the manuscript; or in the decision to publish the results must be declared in this section. If there is no role, please state "The funders had no role in the design of the study; in the collection, analyses, or interpretation of data; in the writing of the manuscript; or in the decision to publish the results".

Appendix A. Derivation of the PDEs in (20)

We exploit the fact that $\epsilon = \dfrac{H_0^\star}{L^\star} \ll 1$ and expand each of the unknowns variables $(u, w, p, \tau^{xx}, \tau^{zz}, \tau^{xz}, h)$ as a power series in ϵ^2 of the form:

$$(u, w, p, \tau^{xx}, \tau^{zz}, \tau^{xz}, \theta) = (u, w, p, \tau^{xx}, \tau^{zz}, \tau^{xz}, \theta)_0(x, z, t) + \epsilon^2 (u, w, p, \tau^{xx}, \tau^{zz}, \tau^{xz}, \theta)_1(x, z, t) + O(\epsilon^4). \quad \text{(A1)}$$

Substituting this into Eqs. (18$(a-n)$. we obtain at $O(1)$:

$$
\begin{aligned}
& u_{0x} + w_{0z} = 0, && \text{(A2)}\\
& \tau_{0z}^{xz} = 0, && \text{(A3)}\\
& -p_{0z} + \tau_{0x}^{xz} + \tau_{0z}^{zz} = 0, && \text{(A4)}\\
& w_0 = u_{0z} = \tau_0^{xz} = 0, \text{ at } z = 0, && \text{(A5)}\\
& -p_0 + \tau_0^{zz} - 2h_x\tau_0^{xz} = \frac{1}{Ca}h_{xx}, \text{ at } z = h && \text{(A6)}\\
& \tau_0^{xz} = 0, \text{ at } z = h. && \text{(A7)}
\end{aligned}
$$

Eqs. (A3), (A5) and (A7) imply that

$$\tau_0^{xz}(x, z, t) = 0. \tag{A8}$$

Integrating Eq. (A4) with respect to z and using Eq. (A5) and (A6), we obtain

$$p_0 = \tau_0^{zz} - \frac{1}{Ca}h_{xx}. \tag{A9}$$

To determine $\tau_0^{xx,zz}$, we need to analyse the $O(\epsilon^2)$ equations. Before we do this, we note the following: $u_{0z} = 0$, so $u_0 = u_0(x, t)$, using $\tau_0^{xz} = 0$ and Eq. (18e) at leading order. In addition, $\tau_0^{zz} = -\tau_0^{xx}$, using Eq. (A2) in Eq. (18e). Eq. (A2) also gives $w_{0z} = -u_{0x}$, which on integrating with respect to z and using $w_0 = 0$ at $z = 0$, gives $w_0(x, z, t) = -u_{0x}z$. At $O(\epsilon^2)$, we have

$$
\begin{aligned}
& Re(u_{0t} + u_0u_{0x} + w_0u_{0z}) = -p_{0x} + \tau_{0x}^{xx} + \tau_{1z}^{xz} + 1, && \text{(A10)}\\
& Re(w_{0t} + u_0w_{0x} + w_0w_{0z}) = -p_{1z} + \tau_{1x}^{xz} + \tau_{1z}^{zz}, && \text{(A11)}\\
& w_1 = u_{1z} = \tau_{1z}^{xz} = 0, \text{ at } z = 0, && \text{(A12)}\\
& \tau_1^{xz} - h_x^2\tau_0^{xz} + h_x(\tau_0^{zz} - \tau_0^{xx}) = -\frac{M}{Ca}[\theta_{0x} + h_x\theta_{0z}], \text{ at } z = h. && \text{(A13)}
\end{aligned}
$$

Integrating Eq. (A10) with respect to z and using Eq. (A12), we obtain

$$\tau_1^{xz} = -2\int_0^z \tau_{0x}^{xx}dz - \left[\frac{1}{Ca}h_{xxx} + 1 - Re(u_{0t} + u_0u_{0x})\right]z. \tag{A14}$$

Substituting this into Eq. (A13) gives

$$2\int_0^h \tau_{0x}^{xx}dz + 2h_x\tau_0^{xx} + h\left[\frac{1}{Ca}h_{xxx} + 1 - Re(u_{0t} + u_0u_{0x})\right] = \frac{M}{Ca}[\theta_{0x} + h_x\theta_{0z}|_{z=h}]. \tag{A15}$$

Eq. (A15) represents the force balance at the free surface of the extensional stress (represented by the first two term), surface tension (represented by the third term), gravity (represented by the fourth term), inertia (represented by the fifth and sixth terms) and variations in surface tension (represented by the last term).

To determine the evolution equation of h using Eq. (18j), we also need to determine u_0 and the $O(\epsilon^2)$ correction u_1. We use the constitutive law to determine these. From Eq. (18e), we obtain

$$
\begin{aligned}
& u_{0x} = \frac{1}{2\mu(\theta_0)}\tau_0^{xx}, && \text{(A16)}\\
& u_{1z} + w_{0x} = \frac{1}{\mu(\theta_0)}\tau_1^{xz} \Rightarrow u_{1z} = \frac{1}{\mu(\theta_0)}\tau_1^{xz} - w_{0x} = \frac{1}{\mu(\theta_0)}\tau_1^{xz} + u_{0xx}z, && \text{(A17)}
\end{aligned}
$$

where $\mu(\theta_0)$ is given by Eq. (18n). We can combine Eqs. (A15) and (A16) to write a single evolution equation for u_0. This can be written as:

$$Re\ h(u_{0t}+u_0u_{0x})-4\left[\mu(\theta_0)h_xu_{0x}+\int_0^h(\mu(\theta_0)u_{0x})_x\,dz\right]=h\left[\frac{1}{Ca}h_{xxx}+1\right]-\frac{M}{Ca}[\theta_{0x}+h_x\theta_{0z}|_{z=h}]. \tag{A18}$$

Finally, the evolution equation for h can be obtained from Eq. (18j) as:

$$h_t+Q_{0x}=0,\ \ Q_0=u_0h. \tag{A19}$$

Hence, Eqs. (A19) and (A18) provide a coupled system of two PDEs for the film's free surface evolution, $h(x,t)$ and the extensional flow speed $u_0(x,t)$, respectively.

Appendix B. Mapping $(x,z)\in[0,1]\times[0,h]$ to a rectangular domain $(x,z)\in[0,1]\times[0,1]$

In order to solve Eqs. (20) numerically, it is instructive to map $(x,z)\in[0,1]\times[0,h]$ to a rectangular domain $(x,z)\in[0,1]\times[0,1]$. We apply the following change of variables:

$$\bar{x}=x,\ \ \bar{z}=\frac{z}{h(x,t)},\ \ \ \bar{t}=t. \tag{A20}$$

Using the chain rule, we can write

$$\frac{\partial}{\partial x}=\frac{\partial}{\partial\bar{x}}-\frac{\bar{z}h_{\bar{x}}}{h}\frac{\partial}{\partial\bar{z}},\quad \frac{\partial}{\partial z}=\frac{1}{h}\frac{\partial}{\partial\bar{z}},\quad \frac{\partial}{\partial t}=\frac{\partial}{\partial\bar{t}}-\frac{\bar{z}h_{\bar{t}}}{h}\frac{\partial}{\partial\bar{z}}. \tag{A21}$$

Applying the above change of variables to Eq. (20d,20e,20f), we obtain the transformed evolution equation for $\theta(\bar{x},\bar{z},\bar{t})$ given by

$$Pe_r\left[\theta_{\bar{t}}+u\theta_{\bar{x}}+(w-\bar{z}uh_{\bar{x}}-\bar{z}h_{\bar{t}})\frac{1}{h}\theta_{\bar{z}}\right]=\frac{1}{h^2}\theta_{\bar{z}\bar{z}}+\epsilon^2\left[\theta_{\bar{x}\bar{x}}-\bar{z}\left(\frac{h_{\bar{x}}}{h}\right)_{\bar{x}}\theta_{\bar{z}}-\frac{\bar{z}h_{\bar{x}}}{h}\left(2\theta_{\bar{x}\bar{z}}-\left(\frac{\bar{z}h_{\bar{x}}}{h}\theta_{\bar{z}}\right)_{\bar{z}}\right)\right],\ (\bar{x},\bar{z})\in[0,1]\times[0,1],$$

$$w(\bar{x},\bar{z},\bar{t})=-u_{\bar{x}}h\bar{z},\ (\bar{x},\bar{z})\in[0,1]\times[0,1], \tag{A22a}$$

$$\theta_{\bar{z}}=0,\ \text{at}\ \bar{z}=0,\ \forall\bar{x}\in[0,1],\ \ \theta_{\bar{z}}=-a\epsilon^2h\theta,\ \text{at}\ \bar{z}=1,\ \forall\bar{x}\in[0,1], \tag{A22b}$$

$$\theta_{\bar{x}}=\epsilon^2b(\theta-\theta_s)+\frac{\bar{z}h_{\bar{x}}}{h}\theta_{\bar{z}},\ \text{at}\ \ \bar{x}=0,\ \forall\bar{z}\in[0,1],\ \ \theta_{\bar{x}}=-\epsilon^2b(\theta-\theta_s)+\frac{\bar{z}h_{\bar{x}}}{h}\theta_{\bar{z}},\ \text{at}\ \ \bar{x}=1,\ \forall\bar{z}\in[0,1]. \tag{A22c}$$

The film thickness evolution, Eq. (20a), and the extensional flow speed evolution, Eq. (20b), in the transformed coordinates become,

$$h_{\bar{t}}+Q_{\bar{x}}=0,\ Q=uh, \tag{A23a}$$

$$Reh(u_{\bar{t}}+uu_{\bar{x}})-4\left[\mu(\theta)h_{\bar{x}}u_{\bar{x}}+\int_0^1(\mu(\theta)u_{\bar{x}})_{\bar{x}}h\,d\bar{z}-\int_0^1\bar{z}h_{\bar{x}}(\mu(\theta)u_{\bar{x}})_{\bar{z}}\,d\bar{z}\right]=h\left[\frac{1}{Ca}h_{\bar{x}\bar{x}\bar{x}}+1\right]-\frac{M}{Ca}\left[\theta_{\bar{x}}+\frac{h_{\bar{x}}}{h}\theta_{\bar{z}}|_{\bar{z}=1}\right]. \tag{A23b}$$

References

1. Alahmadi, H.; Naire, S. Non-Newtonian and viscoplastic models of a vertically aligned thick liquid film draining due to gravity. *Physics of Fluids* **2022**, *34*, 012113.
2. Ashby, M.; Evans, A.; Fleck, N.; Gibson, L.; Hutchinson, J.; Wadley, H. *Metal foams: A design guide*; Butterworth-Heinemann, 2000.
3. Banhart, J. Metal foams: Production and Stability. *Advanced Engineering Materials* **2006**, *8*, 781–794.
4. Briceño-Ahumada, Z.; Mikhailovskaya, A.; Staton, J. The role of continuous phase rheology on the stabilization of edible foams: A review. *Physics of Fluids* **2022**, *34*, 031302.
5. Weaire, D.; Hutzler, S.; Cox, S.; Kern, N.; Alonso, M.; Drenckhan, W. The fluid dynamics of foams. *J. of Physics: Condensed matter* **2003**, *15*, S65–S73.
6. Yang, C.C.; Nakae, H. The effects of viscosity and cooling conditions on the foamability of aluminum alloy. *J. Mat. Proc. Tech.* **2003**, *141*, 202–206.

7. Bhogi, S.; Nampoothiri, J.; Ravi, K.; Mukherjee, M. Influence of nano and micro particles on the expansion and mechanical properties of aluminum foams. *Materials Science and Engineering: A* **2017**, *685*, 131–138. https://doi.org/https://doi.org/10.1016/j.msea.2016.12.127.
8. Cox, S.; Bradley, G.; Weaire, D. Metallic foam processing from the liquid state. *The European Physical Journal Applied Physics* **2001**, *14*. https://doi.org/10.1051/epjap:2001141.
9. Griffiths, R. The Dynamics of Lava Flows. *Annu. Rev. Fluid Mech.* **2000**, *32*, 477–518.
10. Shah, M.; van Steijn, V.; Kleijn, C.; Kreutzer, M. Thermal fluctuations in capillary thinning of thin liquid films. *J. Fluid Mechanics* **2013**, *896*, 1090–1107.
11. Wylie, J.; Huang, H. Extensional flows with viscous heating. *J. Fluid Mechanics* **2007**, *571*, 359–370.
12. He, D.; Wylie, J.; Huang, H.; Miura, R. Extension of a viscous thread with temperature-dependent viscosity and surface tension. *J. Fluid Mechanics* **2016**, *800*, 720–752.
13. Tilley, B.; Bowen, M. Thermocapillary control of rupture in thin viscous fluid sheets. *Journal Fluid Mechanics* **2005**, *541*, 399–408.
14. Bowen, M.; Tilley, B. Thermally induced van der Waals rupture of thin viscous fluid sheets. *Physics of Fluids* **2012**, *24*, 032106.
15. Schwartz, L.; Roy, R. Modeling Draining Flow in Mobile and Immobile Soap Films. *J. Colloid and interface Science* **1999**, *218*, 309–323.
16. Champougny, L.; Rio, E.; Restagno, F.; Scheid, B. The break-up of free films pulled out of a pure liquid bath. *J. Fluid Mechanics* **2016**, *811*, 499–524.
17. Naire, S.; Braun, R.; Snow, S. Limiting cases of gravitational drainage of a vertical free film for evaluating surfactants. *SIAM J. Applied Maths.* **2000**, *61*, 889–913.
18. Naire, S.; Braun, R.; Snow, S. An insoluble surfactant model for a vertical draining free film. *Journal of Colloid Interface Science* **2000**, *230*, 91–106.
19. Naire, S.; Braun, R.; Snow, S. An insoluble surfactant model for a vertical draining free film with variable surface viscosity. *Physics of Fluids* **2001**, *13*, 2492–2502.
20. Braun, R.; Snow, S.; Naire, S. Models for gravitationally-driven free-film drainage. *Journal of Engineering Maths.* **2002**, *43*, 281–314.
21. Balmforth, N.; Craster, R. Dynamics of cooling domes of viscoplastic fluid. *J. Fluid Mech.* **2000**, *422*, 225–248.
22. Tripathi, O.; Singh, D.P.; Dwivedi, V.K.; Agarwal, M. A focused review on aluminum metallic foam: Processing, properties, and applications. *Materials Today: Proceedings* **2021**, *47*, 6622–6627. International Conference on Advances in Design, Materials and Manufacturing, https://doi.org/https://doi.org/10.1016/j.matpr.2021.05.099.
23. Alahmadi, H.N. Non-Newtonian and non-isothermal effects in the gravity-driven draining of a vertically-aligned thin liquid film. PhD thesis, Keele University, 2021.
24. Stewart, P.; Davis, S. Dynamics and stability of metallic foams: network modelling. *Journal of Rheology* **2012**, *56*, 543–574.